



Universidad Autónoma
de Madrid

Biblos-e Archivo
Repositorio Institucional UAM

Repositorio Institucional de la Universidad Autónoma de Madrid

<https://repositorio.uam.es>

Esta es la **versión de autor** del artículo publicado en:
This is an **author produced version** of a paper published in:

Journal of Physical Chemistry C 123.3 (2019): 1866-1873

DOI: <https://doi.org/10.1021/acs.jpcc.8b10810>

Copyright: © 2018 American Chemical Society

El acceso a la versión del editor puede requerir la suscripción del recurso
Access to the published version may require subscription

Structural and Electronic Properties of 3,4,9,10-Perylene Tetracarboxylic Dianhydride on h-BN/Rh(110)

A. J. Martínez-Galera^{*1} and J. M. Gómez-Rodríguez^{1, 2, 3}

**Email:* antonio.galera@uam.es *Phone:* +34.91.497.36.38

¹ *Departamento de Física de la Materia Condensada, Universidad Autónoma de Madrid, E-28049 Madrid, Spain.*

² *Condensed Matter Physics Center (IFIMAC), Universidad Autónoma de Madrid, E-28049 Madrid, Spain.*

³ *Instituto Nicolás Cabrera, Universidad Autónoma de Madrid, E-28049 Madrid, Spain.*

ABSTRACT

The structural and electronic properties of 3,4,9,10-perylene tetracarboxylic dianhydride (PTCDA) adsorbed on h-BN monolayers, grown on the rectangularly packed Rh(110) surface, have been characterized by means of scanning tunneling microscopy (STM) and spectroscopy (STS) in ultrahigh vacuum (UHV). During the earliest stages of growth at room temperature, in contrast to what happens over h-BN monolayers grown on the hexagonally packed Rh(111) surface, molecules are assembled into islands according to a herringbone like structure, similar to that of the (102) plane of bulk PTCDA. STM images acquired close the edges of those islands have revealed the orientation of the molecular assembly with respect to the h-BN/Rh(110) interface. By increasing the coverage, this molecular assembly extends covering the h-BN surface. The effect of extended defects at the h-BN/Rh(110) interface on the structural properties of the PTCDA monolayer grown on top has been investigated. Extended defects coming from the underlying Rh(110) surface, as step edges or dislocations, and those originated in the h-BN layer, as domain boundaries, are found to affect differently to the structure of the molecular layer. High resolution STM images have shown the geometry of the frontier molecular orbitals, that is, the highest occupied molecular orbital (HOMO) and the lowest unoccupied molecular orbital (LUMO). Likewise, differential conductance plots have revealed the local density of states (LDOS) as a function of energy of PTCDA adsorbed on the h-BN/Rh(110) surface. Both the HOMO and LUMO geometries and the LDOS plots have provided important information related to the interaction of PTCDA molecules with h-BN monolayers grown on Rh(110). Finally, the structure of the molecular bilayer has been investigated and compared to that of each of the two polymorphs of bulk PTCDA.

Introduction

Interfaces comprising a 2D layered material and a metal substrate provide excellent platforms for the study of molecular adsorption, since they exhibit a high degree of tunability, which, in turn, can be used to induce systematic changes in their interaction with adsorbates. On the one hand, from a fundamental point of view, the interest of such kind of studies resides in obtaining a deep understanding of the underlying physics and chemistry that governs the adsorption on this kind of complex interfaces, disentangling the respective roles of the 2D layered material and the metal substrate underneath, which, in turn, are affected by their interaction. On the other hand, from an applied point of view, that knowledge is of interest, for instance, for the design of more efficient gas sensors.¹

From the side of the 2D material, the tunability of this kind of interfaces is high since they range from insulators as h-BN,² through semiconductors as some transition metals dichalcogenides,^{3, 4} to excellent electronic conductors as graphene⁵. Nevertheless, the present work is focused on the study of the tunability of the adsorption on these interfaces due to the support. Interestingly, in the case of graphene-metal interfaces, the substrate underneath has proven to play a significant role in the molecular adsorption.⁶⁻⁸ Specifically, it has been found a trend in the diffusion barrier of small adsorbates to be higher with increasing graphene-metal interaction.^{7, 8} For h-BN based interfaces, a similar effect was also observed.⁹ Further demonstration of the influence of the material placed underneath the 2D layer has also been achieved by means of the intercalation of different elements at the interface, providing, in turn, a new way to tune the interaction with adsorbates.¹⁰ For the case of graphene based interfaces, elements as K¹¹, O¹²⁻¹⁵, Cs^{14, 16} or Eu^{14, 17}, have been intercalated and it has been demonstrated that it is possible to induce changes in the strength of the van der Waals interaction with organic adsorbates by using this methodology.¹⁰ In

particular, the intercalation of electropositive elements as Cs or Eu at the Graphene/Ir(111) interface has been found to increase the binding energy of Naphthalene molecules, while the opposite happens when intercalating electronegative ones as O.¹⁰

Concerning the substrate, a degree of freedom to tune the properties of its interface with a 2D layered material is the specific atomic structure of the surface of the former. Recently, it was demonstrated that, for graphene and h-BN monolayers, the crystallography of the metal substrate underneath has a strong influence on the interfacial properties.¹⁸ But how does the choice of the crystalline plane of the surface of the substrate under a 2D material layer affect the properties of organic layers grown on top? Is it possible to tune the properties of molecular adlayers by choosing the orientation of the surface of the support of a 2D material layer?

A possible model adsorbate to study the issue discussed in the previous paragraph is the organic semiconductor 3,4,9,10-perylenetetracarboxylic dianhydride (PTCDA), which can interact in various ways with the surface underneath giving rise to different adsorption configurations ranging from physisorption,^{9, 19-33} through weak chemisorption^{23, 24, 34} to strong chemisorption^{35, 36}. On substrates on which PTCDA is physisorbed, molecules are usually arranged in a herringbone like structure similar to that of the (102) plane of the two molecular bulk phases.^{9, 19-33} On surfaces as the ones of Ag(111) and Cu(111), where PTCDA is weakly chemisorbed, the respective molecular assemblies still exhibit a herringbone like structure but in these cases there is a non-negligible charge transfer between the molecules and the substrate.^{23, 24, 34} However, on other surfaces on which a weak chemisorption has also been reported, a brick wall structure has been found.³⁴ Finally, on surfaces giving rise to a stronger molecule-substrate interaction, PTCDA forms a disordered first layer.³⁵⁻³⁷

Here, to the best of our knowledge, we report on the first study of the adsorption of PTCDA on a 2D layered material grown on a non-hexagonal symmetric surface. The specific interface employed in this study consists in a one atom thick layer of h-BN epitaxially grown on Rh(110). Firstly, the structural properties of the PTCDA monolayer will be described and compared to those previously reported for the adsorption of this molecule on the h-BN/Rh(111) surface. Then, a detailed analysis of the electronic properties of PTCDA after its adsorption on top of that interface will be shown. Finally, the growth of PTCDA multilayers will be discussed.

Experimental

Experiments were performed in an ultrahigh vacuum (UHV) system equipped with a home built variable temperature scanning tunneling (VT-STM) microscope for surface characterization.^{6,38} Rh(110) surfaces were prepared by a cycling procedure of Ar⁺ sputtering at 1 keV followed by annealing at 950 °C in an oxygen partial pressure of 2×10^{-6} Torr. After that, the sample was annealed at 950 °C for 300 s but without supplying O₂ into the chamber. A one atom thick h-BN layer was grown by means of CVD by using borazine (C₃H₆N₃) as precursor. More specifically, the Rh(110) substrate was exposed to 45 L borazine at a partial pressure of 2.5×10^{-8} Torr, while it was annealed at 800 °C. PTCDA was sublimated from a home built sublimation cell while the sample was kept at RT. The deposition rate was calibrated by means of STM images. STM measurements were performed at RT in the constant current mode with the bias voltage applied to the sample. STM data were acquired and analyzed by means of the WSxM software.³⁹

Results and discussion

As a reference, Figure 1a shows a large scale STM image acquired on the pristine h-BN/Rh(110) surface prior to the deposition of PTCDA. Figure 1b displays an atomically resolved STM image acquired on the as prepared h-BN/Rh(110) surface. Both topographs are characterized by the presence of a stripe like moiré pattern with a periodicity of about 1.3 nm. As previously reported by the authors, the h-BN monolayer grown on Rh(110) surfaces is composed of grains, each exhibiting one of two possible rotational domains, which are specular to each other and, hence, isostructural¹⁸. Straightforwardly, both domains, corresponding to relative rotations by angles of around $\pm 34^\circ$ between the h-BN lattice and the [001] direction of the Rh(110) surface underneath, are characterized by an identical moiré pattern. In other words, there is a unique moiré pattern along the interface, which, as previously reported, consists of quasi-one dimensional stripes equally spaced with a separation of 1.3 ± 0.1 nm, that are rotated with respect to the h-BN lattice by an angle of around 21° .¹⁸ A plausible ball model for these equivalent domains is shown in Figure 1c.

A schematics of the PTCDA molecule is shown in Figure 2a. The STM analysis reported here has demonstrated that, after its deposition onto the h-BN/Rh(110) surface, it gives rise to a molecular assembly of high structural perfection (see Figure 2b), which looks like the herringbone structure of the (102) plane of the two PTCDA bulk polymorphs (see Figure 2d). The lattice parameters obtained by averaging over a large number of STM images acquired on the PTCDA monolayer grown on h-BN/Rh(110) are $|b_1| = 19.4 \pm 0.8$ Å and $|b_2| = 12.2 \pm 0.6$ Å, and the angle γ between both unit cell vectors is $92^\circ \pm 3^\circ$. These values agree to a reasonable extent with the structural parameters describing the molecular arrangement in the (102) plane of both PTCDA bulk polymorphs.⁴⁰ A similar molecular assembly of PTCDA has been previously

reported on several surfaces for which the molecule-substrate interaction was found to be weak. For instance, this molecular ordering was found when PTCDA is physisorbed on HOPG^{19-21, 25, 41, 42}, Au(111)^{22-24, 42}, graphene^{25-32,43}, h-BN⁹ and transition metal dichalcogenides^{21, 33} surfaces, as well as on substrates on which it is weakly chemisorbed as it is the case of Ag(111)^{23, 24, 34} and Cu(111)^{23, 24}. Likewise, this herringbone structure has also been observed in PTCDA multilayers.^{36, 37, 44,45}

The epitaxy of this molecular structure with respect to the h-BN/Rh(110) interface underneath has been investigated by means of STM images acquired close to the edges of PTCDA islands formed on samples presenting a submonolayer coverage. Figure 2c shows an STM topograph, where the moiré stripes are resolved in bare areas and the herringbone structure is visible in the molecular island. As observed, the molecular assembly is oriented in such a way that the \bar{b}_2 unit cell vector of the herringbone structure forms a small angle with the moiré stripes of the h-BN/Rh(110) surface. By averaging the measurements of that angle performed on different STM images as the one displayed in Figure 2c, a value of $4^\circ \pm 3^\circ$ is obtained.

Interesting conclusions about the interaction between the PTCDA monolayer and the h-BN/Rh(110) interface can be inferred from Figure 2. First, according to STM images as the one shown in Figure 2b, the lattice parameters of the molecular structure agree to a reasonable extent with those of the (102) plane of bulk PTCDA, which suggests a weak molecule-substrate interaction. In addition, as observed in Figure 2c, the moiré stripes resulting at the h-BN/Rh(111) interface are not visible across the PTCDA islands, suggesting that they do not have a significant influence on the molecular assembly. In turn, it also could provide further evidence that the molecule-substrate interaction is weak. Similarly, neither the moiré patterns resulting on the graphene/Pt(111)³² interface nor those formed on the h-BN/Pt(111)⁹ are visible through PTCDA

monolayers grown on top. In contrast, after the formation of a single layer of PTCDA on, both the h-BN/Rh(111)⁹ and the graphene/Ru(0001)^{28, 30} surfaces, a modulation with the periodicity of the respective moiré patterns formed at the interface of each 2D layered material with its metal support can be observed through the molecular assembly. Likewise, the $22\times\sqrt{3}$ reconstruction of the Au(111) surface is also observed in STM images after the growth of a PTCDA monolayer on top.⁴² It suggests that the molecular ordering remains less affected on the h-BN/Rh(110), h-BN/Pt(111) and graphene/Pt(111) surfaces than on the graphene/Rh(111) and on the h-BN/Rh(111) ones as well as than on the Au(111) surface. However, although all these observations point towards a weak molecule-substrate interaction, the existence of a preferred orientation of the PTCDA adlayer with respect to the h-BN/Rh(110) interface (see Figure 2c) reveals a certain influence of the latter on the structural properties of the molecular assembly.

It is noteworthy that, while, as above mentioned, the moiré pattern of the h-BN/Rh(111) interface appears superimposed to the molecular lattice,⁹ it is not the case for PTCDA monolayers grown on h-BN/Rh(110). In addition, there is a strong preference of PTCDA molecules to be adsorbed on the pores of the moiré superstructure of the h-BN/Rh(111) interface.⁹ As a result, a molecular assembly exhibiting a long range ordering over this interface is only possible after annealing above RT.⁹ In contrast, as observed in Figure 2, such long range ordering of PTCDA on the h-BN/Rh(110) surface is achieved directly after RT deposition. It demonstrates that, not only the composition, but also the crystallography of the underlying metal surface under the h-BN monolayer affects the properties of the molecular adlayer. This fact could be related to a finding reported recently, according to which the corrugation of 2D layered materials, as graphene and h-BN, epitaxially grown on metal supports is affected by the substrate crystallography.¹⁸

On the basis of the experimental findings summarized in Figure 2, a plausible schematic representation of the molecular structure resulting on the h-BN/Rh(110) surface is proposed in Figure 3. Specifically, a coincidence relationship is found to agree with the experimental findings: a herringbone like molecular assembly with two molecules per unit cell, which is defined by \vec{b}_1 and \vec{b}_2 vectors with 20.57 and 13.3 Å magnitude and a relative rotation angle γ of 91.3°, is coincident with a h-BN structure with lattice parameter of 2.51 Å when the angle between the \vec{b}_2 vector and the moiré stripes is 1.9°. In turn, as previously proposed (see Figure 1), the rotation angle of the h-BN lattice with respect to the [001] direction of the underlying metal substrate would be of $\pm 33.7^\circ$ depending on the rotational domain. The angle, between \vec{b}_1 and \vec{b}_2 vectors and the [001] direction of the metal substrate are, respectively, 38.5° and 52.8° . Thus, the relative orientation between \vec{b}_1 vectors of the molecular unit cells on each of the two specular domains of the h-BN/Rh(110) interface should be 77.0° (i.e., two times 38.5°) and that between \vec{b}_2 ones 105.7° (or, equivalently, its supplementary angle 74.3°). As we will see in the next paragraph, these angles between the molecular assemblies of both domains are in good agreement with the ones measured in STM topographs acquired around the boundary between flakes of the two rotational variants of the h-BN/Rh(110) interface underneath. To finish with the issue of the epitaxy of the PTCDA overlayer on the h-BN/Rh(110) surface, according to the schematics presented in Figure 3, the molecular arrangement as referred to the lattice of h-BN, can be described by the following matrix

$$\begin{pmatrix} 9 & 7 \\ -2 & 4 \end{pmatrix}$$

An ubiquitous feature of interfaces based on a two-dimensional material and a metal substrate is the presence of various kinds of extended defects. Therefore, a fully characterization of the structural properties of the PTCDA monolayer grown on top of the h-BN/Rh(110) surface requires the study of the molecular assembly over regions including such defects. First, the influence of defects coming from the metal substrate underneath as step edges or dislocations will be shown. In this regard, Figure 4a shows a representative STM topograph illustrating the possible influence of a monatomic step in the Rh(110) surface on the structure of the molecular assembly. Figure 4b shows an area of a PTCDA monolayer in which a screw dislocation in the Rh(110) substrate is present. In both cases it is observed that the crystalline structure of the PTCDA overlayer remains essentially unperturbed across such extended defects of the h-BN/Rh(110) interface. Now, the way in which extended defects with origin in the h-BN layer, such as domain boundaries, affects the structure of the molecular layer on top will be analyzed. To this end, Figure 4c shows an STM topograph acquired around a boundary between two adjacent h-BN flakes, differently oriented with respect to the Rh(110) substrate, after the growth of a PTCDA monolayer on top. As observed, the molecular assembly is interrupted across the boundary between both flakes. In this case it is also interesting to note that the angle between \vec{b}_1 vectors of the PTCDA adlayer on both domains is of 78° and that between \vec{b}_2 ones 76° , which are in good agreement with the expected values of 77.0° and 74.3° , respectively, extracted from the schematic representation of the molecular assembly displayed in Figure 3.

The behavior of PTCDA monolayers over areas of graphene around extended defects in the underlying substrate has been studied previously for the cases in which graphene was grown on silicon carbide^{25, 26} and on Pt(111)³². In both cases the PTCDA monolayer was found to continue in a carpet-like way, without being significantly perturbed by the presence of step edges in the

underlying substrate, due mainly to the higher molecule-molecule interaction compared to that between molecules and the graphene surface. Consistently, as above mentioned, our study performed on the PTCDA monolayer grown on the h-BN/Rh(110) surface reveals an identical behavior. However, to the best of our knowledge, there is not any analogous systematic study, previously reported, for the case of interfaces between a metal substrate and a 2D material layer around extended defects in the latter as domain boundaries. According to our results, such boundaries in the h-BN monolayers epitaxially grown over Rh(110) substrates interrupt the PTCDA adlayer, in contrast to what happens over areas of this interface around step edges or dislocations in the underlying metal surface.

STS experiments have been carried out in order to extract information on the electronic structure of PTCDA molecules in a monolayer grown on the h-BN/Rh(110) surface. First, by means of bias voltage dependent STM imaging, the frontier orbitals of the molecules in the PTCDA adlayer have been probed. Our data have revealed two kinds of reproducible submolecular features, which are found typically at bias voltages from -2.3 to -2.1 V and from +1.2 to +1.5 V, respectively. Representative STM images of each kind of submolecular features are displayed in Figure 5a,b.

To have a more complete insight on the electronic structure of PTCDA on h-BN/Rh(110), the Local Density of States (LDOS) as a function of energy has been studied by means of differential conductance dI/dV plots. Figure 5c shows a representative dI/dV plot obtained by numerical differentiation of an I/V curve acquired on the PTCDA monolayer grown on the h-BN/Rh(110) surface. As observed in Figure 5c, two peaks centered at around -2.1 and +1.4 V can be clearly distinguished in the differential conductance plot, which is proportional to the LDOS of PTCDA on the h-BN/Rh(110) surface.

The intramolecular features observed in Figure 5a,b resemble, respectively, to the previously reported geometries of the highest occupied molecular orbital (HOMO) and of the lowest unoccupied molecular orbital (LUMO) obtained from DFT calculations carried out for the free molecule in gas phase.⁴² Similar intramolecular features were also observed in PTCDA molecules physisorbed on Au(111)⁴² as well as on graphene/Pt(111),³² graphene/Ru(0001)³⁰ and WSe₂/graphite³³. In all these cases they were ascribed to the HOMO and LUMO. Therefore, it is reasonable to associate the intramolecular features observed in Figure 5a,b to the HOMO and LUMO, respectively, of PTCDA molecules adsorbed on the h-BN/Rh(110) surface. By comparing with the case of PTCDA adsorbed on h-BN epitaxially grown on the hexagonally packed Rh(111) surface,⁹ it should be mentioned that the previously reported geometry of the HOMO is similar to the one shown in Figure 5a, although they were acquired at higher voltages (in absolute values) than those obtained in the present work.

Likewise, LDOS similar to that extracted from the dI/dV plot shown in Figure 5c were reported for PTCDA monolayers weakly coupled to substrates as Au(111),^{42, 33} graphite³³, graphene/SiC(0001),²⁶ graphene/Pt(111)³² and WSe₂/graphite³³. The comparison of the LDOS reported on those substrates with the dI/dV plot displayed in Figure 5c allows to ascribe the two peaks at -2.1 and +1.4 V to the HOMO and LUMO of PTCDA molecules on h-BN epitaxially grown on Rh(110). Additionally, that comparison points towards a weak molecule-substrate interaction also for the PTCDA monolayer grown on h-BN/Rh(110). Finally, from the position with respect to the Fermi level of both peaks observed in the dI/dV plot shown in Figure 5c, it can be concluded that charge transfer between the PTCDA molecules and the h-BN/Rh(110) interface, if any, must be small.

As above mentioned, the geometry and dimensions of the unit cell of PTCDA monolayers grown on h-BN/Rh(110) are in agreement with those previously reported for the (102) molecular plane of the two PTCDA polymorphs. But what happens with the bilayer? Do they grow according to the 3D crystal structure of PTCDA? In order to answer these questions, the structure of the PTCDA bilayer has been studied in the present work. An STM image, where a region partially covered by a PTCDA bilayer is observed, is presented in Figure 6a. A zoom-in over the area marked in black in Figure 6a is also displayed in Figure 6b. As observed, the second layer exhibits a herringbone arrangement with identical unit cell to the first one. Also, it is observed that the molecular assembly of the second layer is aligned with that of the first one. Yellow lines in Figure 6b indicate the stacking direction of the unit cell of the monolayer with respect to the second layer, which should be expected for the α polymorph (i.e. along \bar{b}_1), while blue lines represent those for the case of the β phase (i.e. along \bar{b}_2)⁴⁰. Figure 6b shows that the stacking direction between the first and the second molecular layers grown on the h-BN/Rh(110) surface is, in this case, in agreement with that between (102) planes of the α polymorph of PTCDA. In Figure 6c, a profile along the blue line in Figure 6a is shown. On this profile it is observed that the apparent height of the first PTCDA monolayer with respect to the h-BN surface (darker patch at the lower part of the image) is slightly higher than 3 Å. It is consistent with the distance between (102) planes of PTCDA for both polymorphs.⁴⁶ The same apparent height is roughly found for the second molecular layer with respect to the first one.

Then, the information summarized in Figure 6 is consistent with a 3D structure of PTCDA on the h-BN/Rh(110) surface similar to that of the bulk of PTCDA, at least for the first two layers. This finding is consistent with the conclusions extracted by Huang *et al.*²⁵ and by Emery *et al.*²⁷ for the case of PTCDA overlayers grown on epitaxial graphene on Si-terminated SiC. Nevertheless,

to the best of our knowledge, there are not any previous report describing the structure of PTCDA bilayers on 2D layered materials epitaxially grown on metal substrates.

Conclusions

Here, the structural and electronic properties of PTCDA grown on h-BN/Rh(110) substrates have been studied by means of STM and STS. It has been found that the monolayer grows according to a molecular assembly similar of that of the (102) plane of the two PTCDA bulk polymorphs. A rather different scenario had been previously reported for PTCDA on h-BN monolayers grown on the hexagonally packed Rh(111) surface; the present work, thus, suggests a significant effect of the substrate crystallography on the structural properties of the organic adlayers. In STM images acquired at submonolayer coverages, around the boundary between covered and uncovered areas, an angle between the unit cell vector \vec{b}_2 and the moiré stripes resulting at the h-BN/Rh(110) interface of $4^\circ \pm 3^\circ$ has been measured. With all this information on the structure of the PTCDA monolayer grown on the h-BN/Rh(110) surface, a tentative model of the molecular assembly has been extracted. The crystalline structure of the PTCDA adlayer remains essentially unperturbed by the presence of defects as step edges and dislocations in the underlying Rh(110) substrate, while it is interrupted across domain boundaries in the h-BN monolayer. The geometry of the HOMO and LUMO, as extracted from STM images, and the LDOS, as extracted from differential conductance plots, suggest a weak molecule-substrate coupling for PTCDA monolayers grown on the h-BN/Rh(110) surface. Finally, at higher coverages, STM topographs reveal that the second layer exhibits the same molecular ordering as the first one, and that the

apparent height between both, as measured in STM images, agrees with the distance between (102) planes of the two polymorphs of PTCDA.

ACKNOWLEDGMENT

Financial support from AEI and FEDER under project MAT2016-77852-C2-2-R (AEI/FEDER, UE) and from MINECO under project MDM-2014-0377 is gratefully acknowledged. A.J.M.-G. acknowledges support from the Spanish MINECO through a Juan de la Cierva-Incorporation grant (ref. IJCI-2014-19209).

REFERENCES

- (1) Schedin, F.; Geim, A. K.; Morozov, S. V.; Hill, E. W.; Blake, P.; Katsnelson, M. I.; Novoselov, K. S. Detection of Individual Gas Molecules Adsorbed on Graphene. *Nat. Mater.* **2007**, *6*, 652-655.
- (2) Corso, M.; Auwarter, W.; Muntwiler, M.; Tamai, A.; Greber, T.; Osterwalder, J. Boron Nitride Nanomesh. *Science* **2004**, *303*, 217-220.
- (3) Mak, K. F.; Lee, C.; Hone, J.; Shan, J.; Heinz, T. F. Atomically Thin MoS₂: A New Direct-Gap Semiconductor. *Phys. Rev. Lett.* **2010**, *105*, 136805.
- (4) Wang, Q. H.; Kalantar-Zadeh, K.; Kis, A.; Coleman, J. N.; Strano, M. S. Electronics and Optoelectronics of Two-Dimensional Transition Metal Dichalcogenides. *Nat. Nanotechnol.* **2012**, *7*, 699-712.

- (5) Novoselov, K. S.; Geim, A. K.; Morozov, S. V.; Jiang, D.; Zhang, Y.; Dubonos, S. V.; Grigorieva, I. V.; Firsov, A. A. Electric Field Effect in Atomically Thin Carbon Films. *Science* **2004**, *306*, 666-669.
- (6) Martinez-Galera, A. J.; Gomez-Rodriguez, J. M. Nucleation and Growth of the Prototype Azabenzene 1,3,5-Triazine on Graphite Surfaces at Low Temperatures. *J. Phys. Chem. C* **2011**, *115*, 11089-11094.
- (7) Martinez-Galera, A. J.; Gomez-Rodriguez, J. M. Surface Diffusion of Simple Organic Molecules on Graphene on Pt(111). *J. Phys. Chem. C* **2011**, *115*, 23036-23042.
- (8) Martin-Recio, A.; Martinez-Galera, A. J.; Gomez-Rodriguez, J. M. Surface Diffusion of Azabenzene s-Triazine Molecules on a Strong Interacting Graphene-Metal System. *J. Phys. Chem. C* **2015**, *119*, 401-406.
- (9) Forker, R.; Dienel, T.; Krause, A.; Gruenewald, M.; Meissner, M.; Kirchhübel, T.; Groning, O.; Fritz, T. Optical Transition Energies of Isolated Molecular Monomers and Weakly Interacting Two-Dimensional Aggregates. *Phys. Rev. B* **2016**, *93*, 165426.
- (10) Huttmann, F.; Martinez-Galera, A. J.; Caciuc, V.; Atodiresei, N.; Schumacher, S.; Standop, S.; Hamada, I.; Wehling, T. O.; Bluegel, S.; Michely, T. Tuning the Van der Waals Interaction of Graphene with Molecules Via Doping. *Phys. Rev. Lett.* **2015**, *115*, 236101.
- (11) Gruneis, A.; Vyalikh, D. V. Tunable Hybridization between Electronic States of Graphene and a Metal Surface. *Phys. Rev. B* **2008**, *77*, 193401.
- (12) Martinez-Galera, A. J.; Schroeder, U. A.; Huttmann, F.; Jolie, W.; Craes, F.; Busse, C.; Caciuc, V.; Atodiresei, N.; Bluegel, S.; Michely, T. Oxygen Orders Differently under Graphene: New Superstructures on Ir(111). *Nanoscale* **2016**, *8*, 1932-1943.

- (13) Romero-Muniz, C.; Martin-Recio, A.; Pou, P.; Gomez-Rodriguez, J. M.; Perez, R. Strong Dependence of Flattening and Decoupling of Graphene on Metals on the Local Distribution of Intercalated Oxygen Atoms. *Carbon* **2016**, *101*, 129-134.
- (14) Schroder, U. A.; Petrovic, M.; Gerber, T.; Martinez-Galera, A. J.; Granas, E.; Arman, M. A.; Herbig, C.; Schnadt, J.; Kralj, M.; Knudsen, J.; Michely, T. Core Level Shifts of Intercalated Graphene. *2D Mater.* **2017**, *4*, 015013.
- (15) Romero-Muniz, C.; Martin-Recio, A.; Pou, P.; Gomez-Rodriguez, J. M.; Perez, R. Unveiling the Atomistic Mechanisms for Oxygen Intercalation in a Strongly Interacting Graphene-Metal Interface. *Phys. Chem. Chem. Phys.* **2018**, *20*, 13370-13378.
- (16) Petrovic, M.; Rakic, I. S.; Runte, S.; Busse, C.; Sadowski, J. T.; Lazic, P.; Pletikosic, I.; Pan, Z. H.; Milun, M.; Pervan, P.; Atodiresei, N.; Brako, R.; Sokcevic, D.; Valla, T.; Michely, T.; Kralj, M. The Mechanism of Caesium Intercalation of Graphene. *Nat. Commun.* **2013**, *4*, 2772.
- (17) Schumacher, S.; Wehling, T. O.; Lazic, P.; Runte, S.; Foerster, D. F.; Busse, C.; Petrovic, M.; Kralj, M.; Bluegel, S.; Atodiresei, N.; Caciuc, V.; Michely, T. The Backside of Graphene: Manipulating Adsorption by Intercalation. *Nano Lett.* **2013**, *13*, 5013-5019.
- (18) Martínez-Galera, A. J.; Gómez-Rodríguez, J. M. Influence of Metal Support in-Plane Symmetry on the Corrugation of Hexagonal Boron Nitride and Graphene Monolayers. *Nano Res.* **2018**, *11*, 4643-4653.
- (19) Ludwig, C.; Gompf, B.; Glatz, W.; Petersen, J.; Eisenmenger, W.; Mobus, M.; Zimmermann, U.; Karl, N. Video-STM, LEED and X-Ray-Diffraction Investigations of PTCDA on Graphite. *Z. Phys. B-Condens. Mat.* **1992**, *86*, 397-404.

- (20) Hoshino, A.; Isoda, S.; Kurata, H.; Kobayashi, T. Scanning Tunneling Microscope Contrast of Perylene-3,4,9,10-Tetracarboxylic-Dianhydride on Graphite and Its Application to the Study of Epitaxy. *J. Appl. Phys.* **1994**, *76*, 4113-4120.
- (21) Ludwig, C.; Gompf, B.; Petersen, J.; Strohmaier, R.; Eisenmenger, W. STM Investigations of PTCDA and PTCDI on Graphite and MoS₂ - A Systematic Study of Epitaxy and STM Image-Contrast. *Z. Phys. B-Condens. Mat.* **1994**, *93*, 365-373.
- (22) Fenter, P.; Schreiber, F.; Zhou, L.; Eisenberger, P.; Forrest, S. R. In Situ Studies of Morphology, Strain, and Growth Modes of a Molecular Organic Thin Film. *Phys. Rev. B* **1997**, *56*, 3046-3053.
- (23) Tautz, F. S. Structure and Bonding of Large Aromatic Molecules on Noble Metal Surfaces: The Example of PTCDA. *Prog. Surf. Sci.* **2007**, *82*, 479-520.
- (24) Duhm, S.; Gerlach, A.; Salzmann, I.; Broker, B.; Johnson, R. L.; Schreiber, F.; Koch, N. PTCDA on Au(111), Ag(111) and Cu(111): Correlation of Interface Charge Transfer to Bonding Distance. *Org. Electron.* **2008**, *9*, 111-118.
- (25) Huang, H.; Chen, S.; Gao, X. Y.; Chen, W.; Wee, A. T. S. Structural and Electronic Properties of PTCDA Thin Films on Epitaxial Graphene. *ACS Nano* **2009**, *3*, 3431-3436.
- (26) Wang, Q. H.; Hersam, M. C. Room-Temperature Molecular-Resolution Characterization of Self-Assembled Organic Monolayers on Epitaxial Graphene. *Nat. Chem.* **2009**, *1*, 206-211.
- (27) Emery, J. D.; Wang, Q. H.; Zarrouati, M.; Fenter, P.; Hersam, M. C.; Bedzyk, M. J. Structural Analysis of PTCDA Monolayers on Epitaxial Graphene with Ultra-High Vacuum Scanning Tunneling Microscopy and High-Resolution X-Ray Reflectivity. *Surf. Sci.* **2011**, *605*, 1685-1693.

- (28) Roos, M.; Uhl, B.; Kuenzel, D.; Hoster, H. E.; Gross, A.; Behm, R. J. Intermolecular vs Molecule-Substrate Interactions: A Combined STM and Theoretical Study of Supramolecular Phases on Graphene/Ru(0001). *Beilstein J. Nanotechnol.* **2011**, *2*, 365-373.
- (29) Wang, Q. H.; Hersam, M. C. Nanofabrication of Heteromolecular Organic Nanostructures on Epitaxial Graphene via Room Temperature Feedback-Controlled Lithography. *Nano Lett.* **2011**, *11*, 589-593.
- (30) Zhou, H. T.; Mao, J. H.; Li, G.; Wang, Y. L.; Feng, X. L.; Du, S. X.; Muellen, K.; Gao, H. J. Direct Imaging of Intrinsic Molecular Orbitals Using Two-Dimensional, Epitaxially-Grown, Nanostructured Graphene for Study of Single Molecule and Interactions. *Appl. Phys. Lett.* **2011**, *99*, 153101.
- (31) Johns, J. E.; Karmel, H. J.; Alaboson, J. M. P.; Hersam, M. C. Probing the Structure and Chemistry of Perylenetetracarboxylic Dianhydride on Graphene before and after Atomic Layer Deposition of Alumina. *J. Phys. Chem. Lett.* **2012**, *3*, 1974-1979.
- (32) Martinez-Galera, A. J.; Nicoara, N.; Martinez, J. I.; Dappe, Y. J.; Ortega, J.; Gomez-Rodriguez, J. M. Imaging Molecular Orbitals of PTCDA on Graphene on Pt(111): Electronic Structure by STM and First-Principles Calculations. *J. Phys. Chem. C* **2014**, *118*, 12782-12788.
- (33) Zheng, Y. J.; Huang, Y. L.; Chenp, Y.; Zhao, W.; Eda, G.; Spataru, C. D.; Zhang, W.; Chang, Y.-H.; Li, L.-J.; Chi, D.; Quek, S. Y.; Wee, A. T. S. Heterointerface Screening Effects between Organic Monolayers and Monolayer Transition Metal Dichalcogenides. *ACS Nano* **2016**, *10*, 2476-2484.
- (34) Glockler, K.; Seidel, C.; Soukopp, A.; Sokolowski, M.; Umbach, E.; Bohringer, M.; Berndt, R.; Schneider, W. D. Highly Ordered Structures and Submolecular Scanning Tunnelling

Microscopy Contrast of PTCDA and DM-PBDCI Monolayers on Ag(111) and Ag(110). *Surf. Sci.* **1998**, *405*, 1-20.

(35) Hirose, Y.; Forrest, S. R.; Kahn, A. Quasiepitaxial Growth of the Organic Molecular Semiconductor 3,4,9,10-Perylenetetracarboxylic Dianhydride. *Phys. Rev. B* **1995**, *52*, 14040-14047.

(36) Martinez-Galera, A. J.; Wei, Z.; Nicoara, N.; Brihuega, I.; Gomez-Rodriguez, J. M. PTCDA Growth on Ge(111)-c(2 x 8) Surfaces: A Scanning Tunneling Microscopy Study. *Nanotechnology* **2017**, *28*, 095703.

(37) Nicoara, N.; Custance, O.; Granados, D.; Garcia, J. M.; Gomez-Rodriguez, J. M.; Baro, A. M.; Mendez, J. Scanning Tunnelling Microscopy and Spectroscopy on Organic PTCDA Films Deposited on Sulfur Passivated GaAs(001). *J. Phys.-Condes. Matter* **2003**, *15*, S2619-S2629.

(38) Custance, O.; Brochard, S.; Brihuega, I.; Artacho, E.; Soler, J. M.; Baró, A. M.; Gómez-Rodríguez, J. M. Single Adatom Adsorption and Diffusion on Si(111)-(7x7) Surfaces: Scanning Tunneling Microscopy and First-Principles Calculations. *Phys. Rev. B* **2003**, *67*, 235410.

(39) Horcas, I.; Fernandez, R.; Gomez-Rodriguez, J. M.; Colchero, J.; Gomez-Herrero, J.; Baro, A. M. WSxM: A Software for Scanning Probe Microscopy and a Tool for Nanotechnology. *Rev. Sci. Instrum.* **2007**, *78*, 013705.

(40) Krause, B.; Durr, A. C.; Ritley, K.; Schreiber, F.; Dosch, H.; Smilgies, D. Structure and Growth Morphology of an Archetypal System for Organic Epitaxy: PTCDA on Ag(111). *Phys. Rev. B* **2002**, *66*, 235404.

(41) Kendrick, C.; Kahn, A.; Forrest, S. R. STM Study of the Organic Semiconductor PTCDA on Highly-Oriented Pyrolytic Graphite. *Appl. Surf. Sci.* **1996**, *104*, 586-594.

- (42) Nicoara, N.; Roman, E.; Gomez-Rodriguez, J. M.; Martin-Gago, J. A.; Mendez, J. Scanning Tunneling and Photoemission Spectroscopies at the PTCDA/Au(111) Interface. *Org. Electron.* **2006**, *7*, 287-294.
- (43) Alaboson, J. M. P.; Wang, Q. H.; Emery, J. D.; Lipson, A. L.; Bedzyk, M. J.; Elam, J. W.; Pellin, M. J.; Hersam, M. C. Seeding Atomic Layer Deposition of High-K Dielectrics on Epitaxial Graphene with Organic Self-Assembled Monolayers. *ACS Nano* **2011**, *5*, 5223-5232.
- (44) Kendrick, C.; Kahn, A. Epitaxial Growth and Phase Transition in Multilayers of the Organic Semiconductor PTCDA on InAs(001). *J. Cryst. Growth* **1997**, *181*, 181-192.
- (45) Kilian, L.; Umbach, E.; Sokolowski, M. Molecular Beam Epitaxy of Organic Films Investigated by High Resolution Low Energy Electron Diffraction (SPA-LEED): 3,4,9,10-Perylenetetracarboxylicacid-Dianhydride (PTCDA) on Ag(111). *Surf. Sci.* **2004**, *573*, 359-378.
- (46) Forrest, S. R. Ultrathin Organic Films Grown by Organic Molecular Beam Deposition and Related Techniques. *Chem. Rev.* **1997**, *97*, 1793-1896.

FIGURES

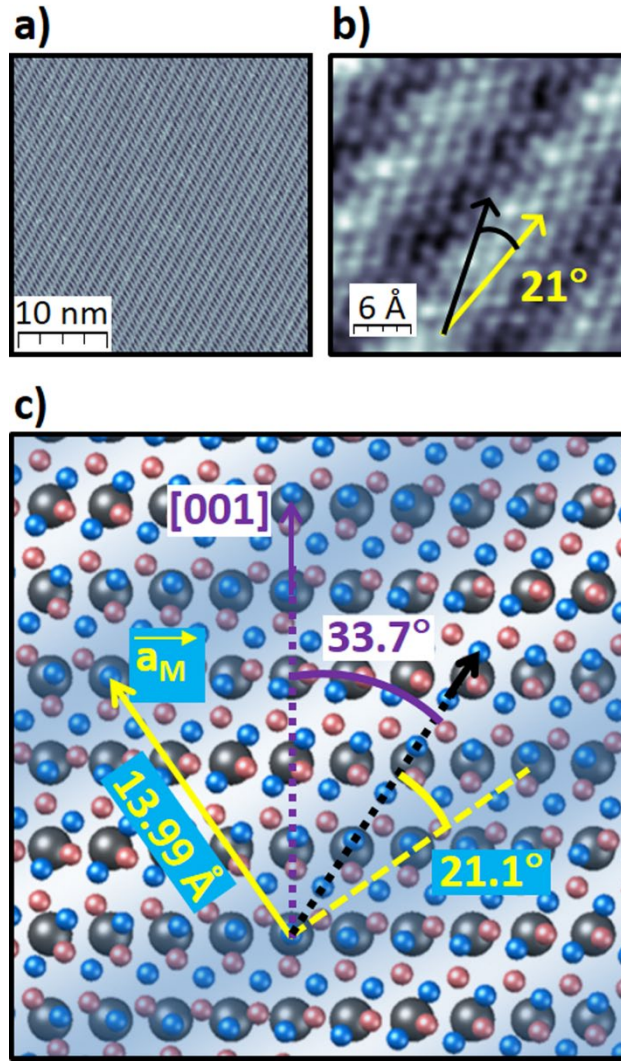


Figure 1. Structure of the h-BN/Rh(110) interface. **a)** Representative STM image acquired on a single layer of h-BN epitaxially grown on top of a Rh(110) substrate. **b)** Atomically resolved STM topograph acquired on the h-BN/Rh(110) interface. The yellow arrow indicates the direction of the moiré stripes and the black one that of the h-BN lattice. **c)** Plausible schematic representation of a rotational domain according to which the h-BN layer would be rotated by $+33.7^\circ$ with respect to the [001] substrate direction, that is indicated by the purple arrow. In turn, the black arrow indicates the direction of the h-BN lattice. The yellow dashed line indicates the

direction of the moiré stripes, while the yellow arrow corresponds to the moiré vector. Note that, here, the sign criterion for the angle of the rotational domains has been chosen as follows: positive for counterclockwise rotation with respect to the [001] direction of the substrate. The rotational domain in which the h-BN layer would be rotated by -33.7° referred to the [001] substrate direction would be just a specular reflection, with respect to that crystallographic direction of Rh(110), of the domain rotated by 33.7° . Tunneling parameters: a) $V_s = +1.32$ V, $I_t = 0.1$ nA; size: 35×35 nm², b) $V_s = +1.37$ V, $I_t = 0.4$ nA; size: 3×3 nm².

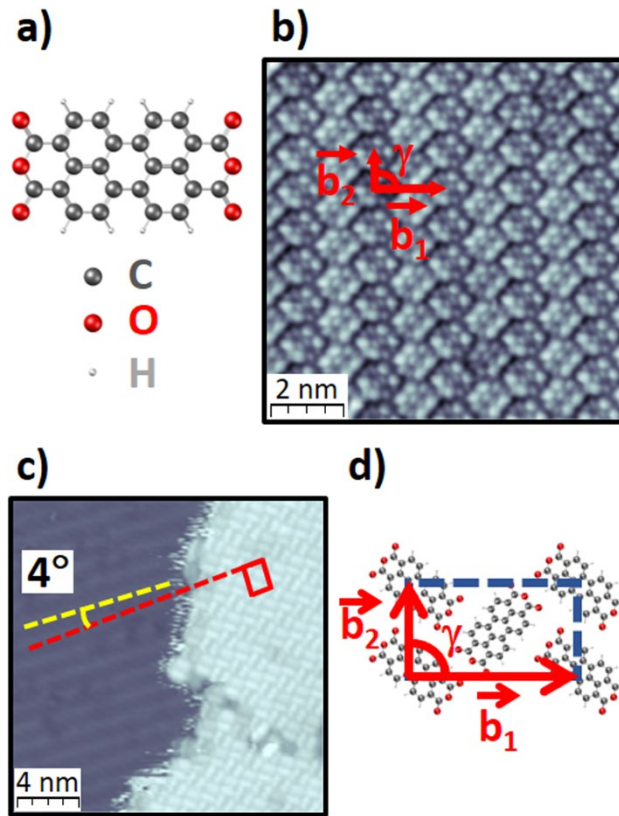


Figure 2. Structure of the PTCDA monolayer grown on h-BN/Rh(110). **a)** Schematic drawing of the PTCDA molecule. **b)** STM topograph acquired after the deposition of a PTCDA overlayer on

the h-BN/Rh(110) interface. The unit cell of the molecular assembly as defined by \vec{b}_1 and \vec{b}_2 vectors and their relative angle, γ , are indicated in red. **c)** STM image acquired in the surroundings of a boundary between a region covered by molecules and another of pristine h-BN/Rh(110) after the growth of an incomplete PTCDA adlayer. The direction of the moiré stripes of the h-BN/Rh(110) interface is indicated by a yellow dashed line and that of the unit cell vector \vec{b}_2 of the PTCDA adlayer by a red one. **d)** Schematic representation of the unit cell of the herringbone structure of PTCDA. Tunneling parameters: b) $V_s = +1.2$ V, $I_t = 0.7$ nA; size: 9.5×9.5 nm², c) $V_s = +1.5$ V, $I_t = 0.05$ nA; size: 20×20 nm².

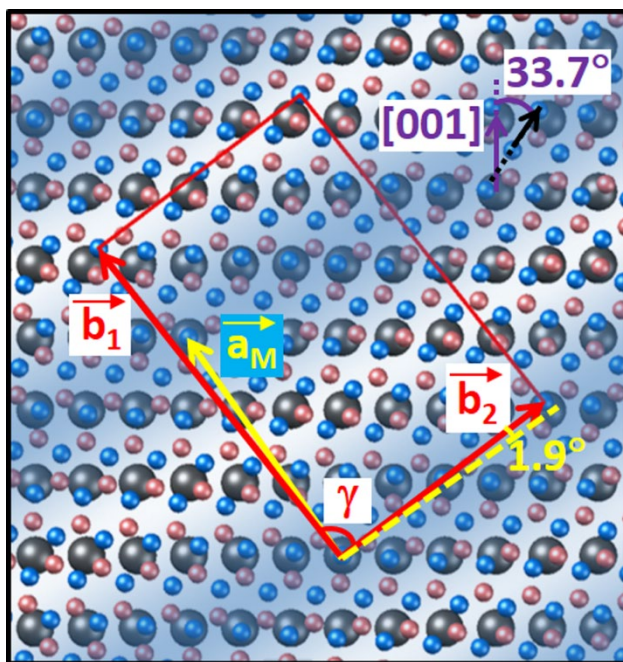


Figure 3. Tentative schematic representation of the molecular assembly on the rotational domain of the h-BN/Rh(110) interface in which the h-BN layer would be rotated by 33.7° with respect to the $[001]$ substrate direction indicated by the purple arrow. The unit cell is a parallelogram,

whose \vec{b}_2 vector is rotated by 1.9° with respect to the moiré stripes that are indicated by a yellow dashed line perpendicular to the moiré vector (yellow arrow). The moduli of \vec{b}_1 and \vec{b}_2 are 20.57 Å and 13.3 Å, respectively, and the angle, γ , is 91.3° . The two molecules within the unit cell have been omitted in the schematics for simplicity. The PTCDA overlayer on the other rotational domain of the h-BN/Rh(110) interface would be an specular reflection with respect to the Rh [001] direction of that displayed in Figure 3.

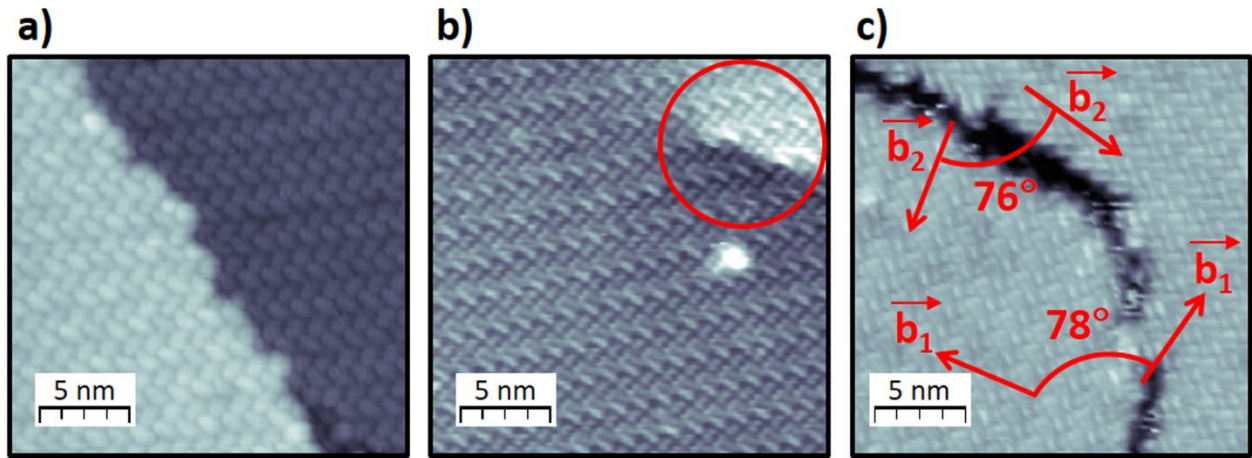


Figure 4. PTCDA overlayer close to extended defects in the h-BN/Rh(110) interface. **a)** and **b)** STM topographs illustrating that the molecular ordering is not perturbed by a) step edges and b) dislocations (see circle) in the Rh(110) substrate under the h-BN layer. **c)** STM image acquired close to the boundary between two rotational domains of the h-BN/Rh(110) interface after the growth of a PTCDA overlayer. As observed, the molecular layer is interrupted along the domain boundary. The angle between the \vec{b}_1 vectors of both cells is 78° and that between the \vec{b}_2 ones is 76° , which are in good agreement with the angles between the respective unit cell vectors of PTCDA on both domains of h-BN extracted from the schematics presented in Figure 3.

Tunneling parameters: a) $V_s = +2.07$ V, $I_t = 0.6$ nA; size: 20×20 nm², b) $V_s = +1.24$ V, $I_t = 0.3$ nA; size: 20×20 nm² and c) $V_s = +1.2$ V, $I_t = 0.4$ nA, size: 20×20 nm².

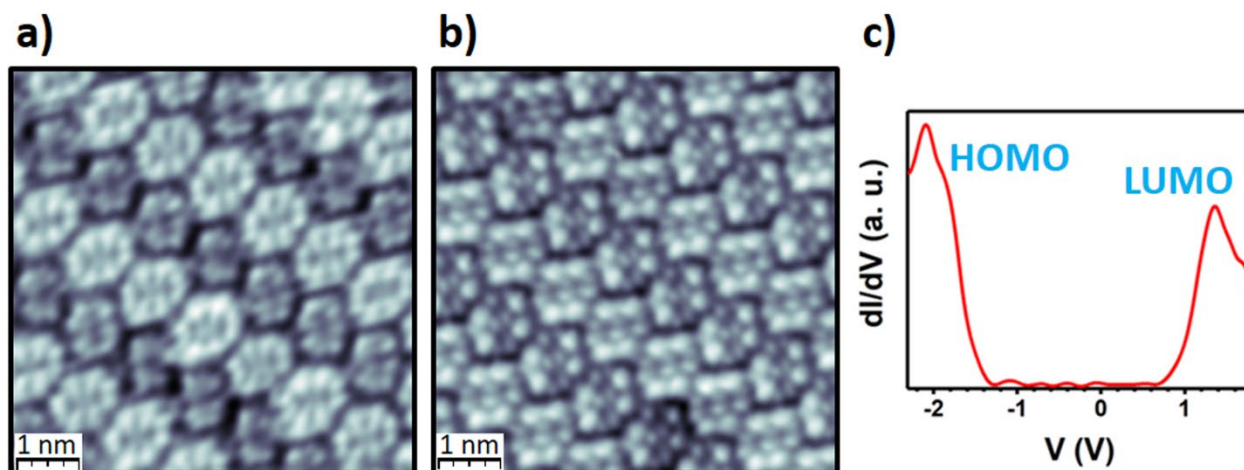


Figure 5. STM study of the electronic structure of PTCDA on the h-BN/Rh(110) interface. **a)-b)** STM images with intramolecular resolution revealing the geometry of the a) highest occupied molecular orbital (HOMO) and b) lowest unoccupied molecular orbital (LUMO) of PTCDA molecules adsorbed on h-BN/Rh(110). **c)** Representative dI/dV spectrum obtained by numerical differentiation of an I/V trace resulting from the average of three curves consecutively acquired at RT by STS on the same region of a PTCDA monolayer grown on top of h-BN/Rh(110). Each one of these three curves contains 256 points, being each the average of forty values consecutively measured. Tunneling parameters: a) $V_s = -2.2$ V, $I_t = 0.084$ nA; size: 6.3×6.3 nm², b) $V_s = +1.2$ V, $I_t = 0.7$ nA; size: 6.3×6.3 nm².

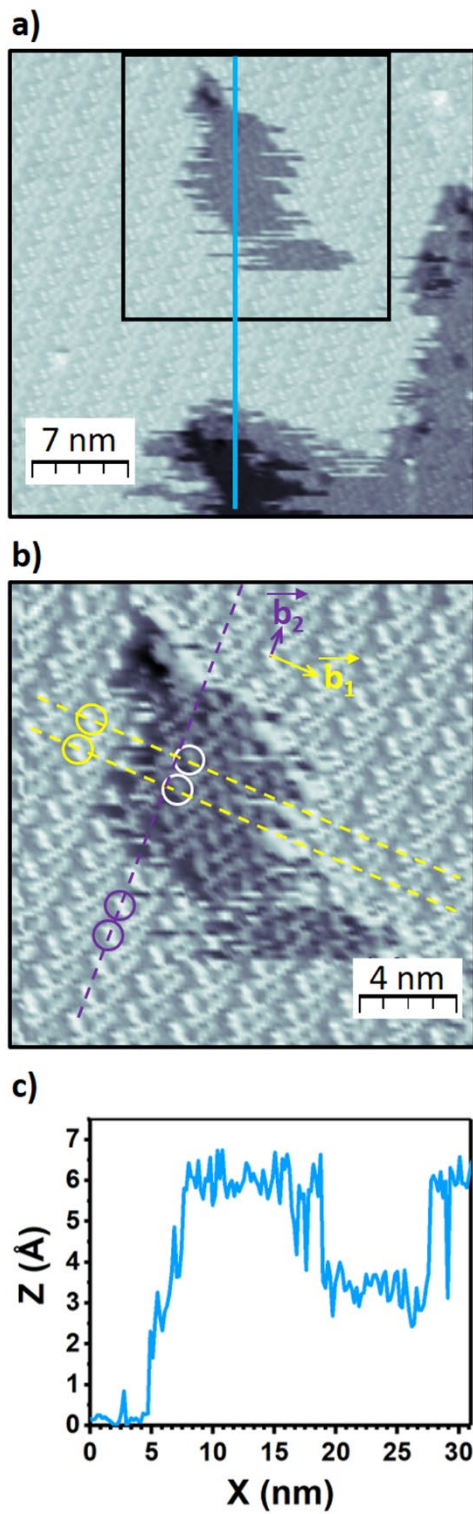


Figure 6. Structural characterization of the PTCDA bilayer on h-BN/Rh(110). **a)** STM image showing a region partially covered by a second layer of PTCDA. The darker patch at the lower

part of the image is a region of the h-BN surface uncovered by molecules. **b)** zoom-in of the area within the square indicated in Figure 6a. Yellow and purple dashed lines indicate, respectively, the direction of \vec{b}_1 and \vec{b}_2 vectors of the molecular unit cell of the second layer. A shift along the direction of \vec{b}_1 is observed in the unit cell of the second layer with respect to that of the first one, in agreement with the stacking direction of the (102) plane for the α phase of bulk PTCDA. **c)** Topography profile along the blue line highlighted in Figure 6a, where it is observed that the apparent height of the second layer with respect to the first one is consistent with the distance between (102) planes of bulk PTCDA. Tunneling parameters: a) $V_s = +1.4$ V, $I_t = 0.6$ nA; size: 32×32 nm², b) size: 19×19 nm².

TOC IMAGE

